On estimating functional average breakthrough curve using time-warping technique and perturbation approach

Zhiming Lu[1] and Philip H. Stauffer[1]

Received 14 October 2011; revised 13 March 2012; accepted 31 March 2012; published 22 May 2012.

[1] Simulated contaminant breakthrough curves (BTC) are often used to predict mass arrival at compliance boundaries at waste storage sites. In numerical simulations that involve uncertainties on input parameters such as randomly heterogeneous rock properties, Monte Carlo simulations are commonly utilized and the mean breakthrough curve is often calculated from the arithmetic average of all realizations. The arithmetic mean breakthrough curve in general overestimates the mass flow rate at early and late time but underestimates the peak mass flow rate. The averaged breakthrough curve usually does not resemble any of individual breakthrough curves. The reason is that BTCs vary not only on amplitude but also on dynamics (time) and therefore it is not appropriate to take the arithmetic average directly. In this study, we consider each BTC as a random curve, and use time-warping techniques to align all curves in a time-warped space, compute the sample mean of the curves in the time-warped space, and transform the means back to the original time space. We show that all BTCs are aligned based on the percentile of mass reaching the compliance boundary, and the functional average is the percentile average of all BTCs. The confidence interval of the sample mean curve is estimated using the perturbation approach. The functional average provides an additional metric that can be used to characterize the breakthrough behavior in addition to more traditional median and arithmetic average curves. The method is illustrated using transport simulations at the Material Disposal Area G, Los Alamos National Laboratory (LANL) in New Mexico.

Citation: Lu, Z., and P. H. Stauffer (2012), On estimating functional average breakthrough curve using time-warping technique and perturbation approach, *Water Resour. Res.*, *48*, W05541, doi:10.1029/2011WR011506.

1. Introduction

[2] Monte Carlo simulation (MCS) is widely used in simulating flow and transport in field-scale applications and in numerically validating stochastic theories. MCS involves generating a large number of realizations, solving the flow or transport problem with each generated parameter realization, and computing statistics of the solutions over all realizations. These statistics are calculated using direct arithmetic "averaging," either with equal weights for equal probable realizations in conventional MCS or different weights for bias-sampled realizations in importance sampling MCS [*Lu and Zhang*, 2003a]. It is well known that the arithmetic average is the best linear unbiased estimator (BLUE) when L_2 norm, which is based on the method of least squares, is used to measure the distance between elements in the sample space, but L_2-norm is sensitive to outliers [*Lin and Li*, 2007; *Bektas and Sisman*, 2010].

[3] Arithmetic averaging has been widely and successfully used in groundwater hydrology to approximate the ensemble mean of some quantities, such as hydraulic head. However, it may not be appropriate to approximate the ensemble mean of some other quantities, for example, breakthrough curves, although it has typically been utilized in the literature to calculate the mean breakthrough curve [*Hu et al.*, 2004; *Zhang et al.*, 2007; *Govindaraju and Das*, 2007; *Riva et al.*, 2008; *Pan et al.*, 2009; *Dai et al.*, 2009]. The mean breakthrough curve computed from arithmetic averaging in general overestimates the mass flow rate at earlier time (early arrival) and later time (long tailing), but it underestimates the mass flow rate at intermediate time. More importantly, it may underestimate the peak mass flow rate, which may be very critical for some hydrologic applications. *Hu et al.* [2004] observed similar differences between results from their stochastic model and MCS, and ascribed these differences to the first-order accuracy of the stochastic model and insufficient realizations of MCS.

[4] However, such differences may stem from improper calculation of the mean breakthrough curve from MCS. As an example, Figure 1a illustrates two normalized cumulative breakthrough curves, C_1 and C_2, and their arithmetic average. The arithmetically averaged curve has a different pattern from the two original breakthrough curves. The mass flow rate corresponding to these two breakthrough curves, as well as their arithmetic average, are shown in Figure 1b. It is noted that the averaged mass flow rate has two peaks, which is not reasonable, because both original curves have a single peak. The reason for disagreement in

[1]Computational Earth Sciences Group (EES-16), Los Alamos National Laboratory, Los Alamos, New Mexico, USA.

©2012. American Geophysical Union. All Rights Reserved.
0043-1397/12/2011WR011506

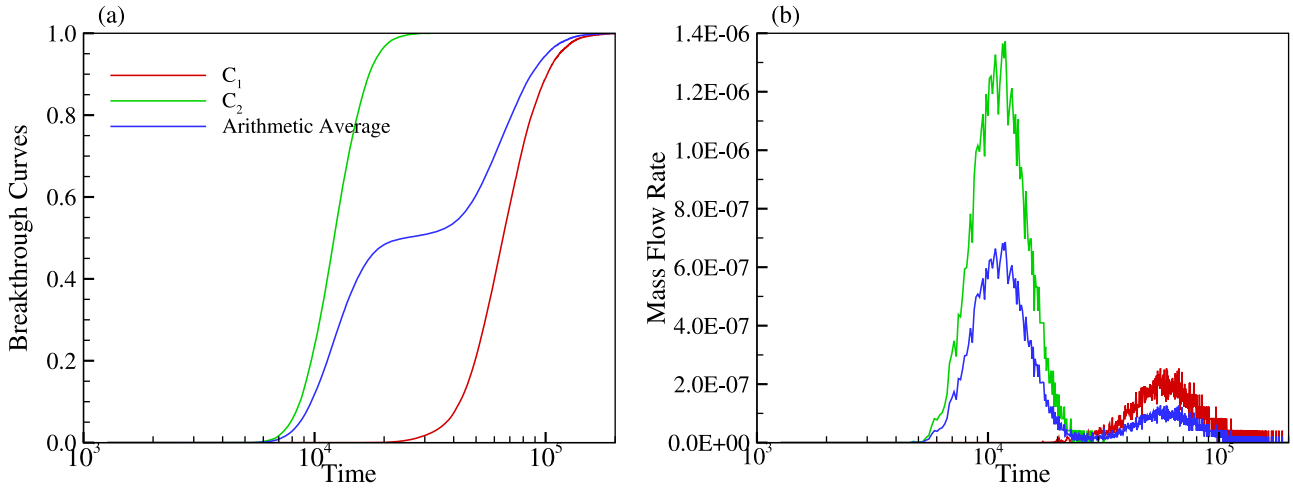

Figure 1. Illustrative example showing the mean breakthrough curve computed from two (a) cumulative and (b) instantaneous breakthrough curves using arithmetic averaging.

the pattern between the arithmetic average and the original breakthrough curves is that the breakthrough curves vary in shape (both amplitude and time progression), and it has been shown that the pointwise arithmetic mean is an inadequate estimate of the mean curve if the curves vary in both amplitude and time progression [*Gasser et al.*, 1984; *Kneip and Gasser*, 1992; *Wang and Gasser*, 1997, 1999].

[5] Several methods have been proposed to deal with random curves, and most of these methods are based on the concept of time warping. Time warping (or curve alignment, time synchronization) is a technique that warps the time axis so that each warped individual curve approximately coincides with the mean behavior of the ensemble of curves. The structure averaging method [*Kneip and Gasser*, 1992] aligns each individual curve to the average location of common features (peaks, troughs, inflection points) observed in sample curves. In the time-shift model of *Silverman* [1995] each individual curve is considered as the result of a random time shift. *Liu and Muller* [2004] treated each observed curve as a realization of a bivariate random process with one component for the random time-warping function and the other for a random amplitude function, and derived the functional mean curve and its confidence intervals. They proved several important properties of the functional average, including the variance-minimizing property and some asymptotic properties.

[6] In this study, we provide an alternative way to derive the functional mean curves and confidence intervals using the combination of the time-warping technique and the perturbation approach. We further prove that, by defining the transformation function as the integral of the original BTC normalized by the area under the curve, the functional average is indeed the percentile average. This work differs from that of *Liu and Muller* [2004] in two aspects. First, by recognizing that the forward transformation function is a cumulative distribution function and that the time-warping function (the inverse of the forward transformation function) is a quantile (or percentile) function, we show that the functional average in this case is, in fact, a percentile averaging, which has very clear physical meaning. Second, our derivation is more concise by using the combination of the time-warping technique and the perturbation approach. The applicability of the methodology is demonstrated using breakthrough curves from Monte Carlo transport simulations for the Material Disposal Area G at Los Alamos National Laboratory, Los Alamos, New Mexico.

2. Mathematical Formulation

[7] Suppose we observed (simulated) a number of (instantaneous) breakthrough curves (also called the *residence time distribution*) $\tilde{C}_i(t_{ij})$, $i = \overline{1, M}$, $j = \overline{1, n_i}$, at certain compliance boundaries in Monte Carlo transport simulations, where M is the number of curves, and n_i is the number of observed values on the i-th curve, and t_{ij} is the observation time for i-th curve at j-th time. With no loss of generality, we assume that all curves are observed at the same N times t_j, $j = \overline{1, N}$ (otherwise, one may interpolate curves such that all curves have observed values at the same discrete observation times). One simple way, which is often used in the literature, to obtain the mean breakthrough curve is by averaging all of these breakthrough curves $\langle C(t) \rangle \approx \sum_{m=1}^{M} \tilde{C}_m / M$. As stated previously, this pointwise average or the cross-sectional average of curves is not a good estimate because these curves vary in both time and amplitude [*Gasser et al.*, 1984; *Kneip and Gasser*, 1992; *Wang and Gasser*, 1997].

[8] We start by following *Liu and Muller* [2004] and consider each observed (or simulated) curve as a stochastic process taking from the space of the observed process (curves)

$$W = \{(t, \tilde{Y}[t], t \in [0, T])\} \subset L^2([0, T]) \times L^2([0, T]), \qquad (1)$$

where $t \in [0, T]$ is the absolute time, $\tilde{Y}(t)$ is the observed curve, and $L^2[0, T]$ is the space of the square integrable functions. Any observed process $(t, \tilde{Y}[t], t \in [0, T]) \in W$ can be considered as a realization generated from a bivariate stochastic process

$$S = \{(X[\tau], Y[\tau]), \tau \in [0, 1]\} \subset L^2([0, 1]) \times L^2([0, 1]), \qquad (2)$$

where $\tau \in [0, 1]$ is referred to as synchronized time or warped time, S the synchronized time space (or time-warped space), and $X(\tau)$ is called the time-warping transformation function, which is an invertible monotonic increasing function that maps the synchronized time $\tau \in [0, 1]$ back to the absolute time $t \in [0, T]$. $Y(\tau)$ can be interpreted as a random amplitude function. As long as $Y(\tau)$ is single-valued (i.e., for any τ, $Y(\tau)$ has a single value) and $X(\tau)$ is an invertible monotonic increasing function, any pair of realizations of $X(\tau)$ and $Y(\tau)$ uniquely determine one realization of $(t, \tilde{Y}[t])$ in the observed time space as,

$$\tilde{Y}(t) = Y(X^{-1}[t]), \quad \forall t \in [0, T]. \tag{3}$$

Conversely, mapping from W to S is nonunique, i.e., for any observed curve $(t, \tilde{Y}[t]) \in W$, there may be many different ways to derive $(X[\tau], Y[\tau]) \in S, \tau \in [0, 1]$.

[9] To better understand the idea of the functional average, we take the geometric mean of the log hydraulic conductivity as an example because the concept is the same. It is well accepted that hydraulic conductivity K_s in a single lithofacies follows a lognormal distribution. If we take M hydraulic conductivity measurements, $K_{s,i}$, we usually do not use their arithmetic mean $K_A = (1/M)\sum_{i=1}^{M} K_{s,i}$. Instead, we take the logarithm transformation of these measurements, $f_i = \ln(K_{s,i})$, calculate the arithmetic mean of the log-transformed values $\langle f \rangle = (1/M)\sum_{i=1}^{M} f_i$, and then find the geometric mean of the hydraulic conductivity by back transformation $K_G = e^{\langle f \rangle}$. It should be noted that the geometric mean depends on the mean of the log-transformed variable only and it is not the same as $\langle e^f \rangle = e^{\langle f \rangle + \sigma_f^2/2}$ (σ_f^2 is the variance of log conductivity), which is the arithmetic mean. Similarly, the functional averaging procedure includes three steps: time-warping (or time-synchronizing) the curves, which transforms all curves to the time-warped space, averaging the time-warped curves in the time-warped space, and transforming the means back to the original time domain using the mean curves in the time-warped space.

2.1. Time Warping

[10] The purpose of time warping is to align curves, which is accomplished by a forward time transformation, denoted as $\tau = \Phi_{\tilde{Y}}(t) : [0, T] \to [0, 1]$. The subscript $\tilde{Y}(t)$ in $\Phi_{\tilde{Y}}(t)$ implies the dependence of this mapping function on observed curve $\tilde{Y}(t)$. In other words, a different mapping function is used for a different observed curve. This function maps absolute time $t \in [0, T]$ to warped time $\tau \in [0, 1]$, and must be monotonically increasing. One example of the forward transformation function is [*Liu and Muller*, 2004]

$$\Phi_{\tilde{Y},p}(t) = \left[\frac{\int_0^t [\tilde{Y}(t)]^p dt}{\int_0^T [\tilde{Y}(t)]^p dt} \right]^{1/p}, \tag{4}$$

where $p > 0$ is a parameter that weighs the importance of the peaks of the curve. However, the physical meaning of this transformation is not clear unless $p = 1$.

[11] For any breakthrough curve $\tilde{Y}(t)$, we assume that $\int_0^T \tilde{Y}(t)dt > 0$, or otherwise one may need either to increase the value of T such that this condition is satisfied or to exclude this realization if there is no mass reaching the compliance boundary at the timescale of interest. We scale the breakthrough curve by the area under the curve:

$$\phi_{\tilde{Y}}(t) = \frac{\tilde{Y}(t)}{\int_0^T \tilde{Y}(t)dt}, \tag{5}$$

and note that this function satisfies $\phi_{\tilde{Y}}(t) \geq 0$, and $\int_0^T \phi_{\tilde{Y}}(t)dt = 1$, which means that this function can be considered as a probability density function. We define the forward transformation function as,

$$\Phi_{\tilde{Y}}(t) = \int_0^t \phi_{\tilde{Y}}(t')dt', \tag{6}$$

which is a cumulative distribution function. In particular, for instantaneous breakthrough curves, one has $\int_0^T \tilde{Y}(t)dt \equiv 1$, and the transformation becomes $\Phi_{\tilde{Y}}(t) = \int_0^t \tilde{Y}(t)dt$, which is the cumulative breakthrough curve.

[12] The time-warping transformation function $X(\tau)$ can be chosen as the inverse of $\Phi_{\tilde{Y}}(t)$:

$$X(\tau) = \Phi_{\tilde{Y}}^{-1}(\tau) = \inf_{t \in [0,T]} \{\Phi_{\tilde{Y}}(t) \geq \tau\}, \tag{7}$$

and the amplitude of the curve is

$$Y(\tau) = \tilde{Y}(X[\tau]), \tag{8}$$

where for simplicity the subscript $\tilde{Y}$ in X and Y has been dropped (unless otherwise confusion may occur), but the dependence of these two functions on $\tilde{Y}$ is implied.

[13] The transformation function $\Phi_{\tilde{Y}}(t)$ in (6) is a special case of (4) at $p = 1$. However, by recognizing that it is a cumulative distribution function, now it has a clear physical meaning, i.e., the percentage of the cumulative mass arrived at the compliance boundary at time t. Since $\Phi(t)$ is a cumulative distribution function, its inverse $X(\tau)$ is called the quantile function or percent point function in statistics. For any $\tau_0 \in [0, 1]$, $X_{\tilde{Y}}(\tau_0)$ is the $(100\tau_0)$ percentile of the travel time distribution for the corresponding breakthrough curve $\tilde{Y}(t)$. For instance, $X_{\tilde{Y}}(0.5)$ is the median (50th percentile) of the travel time distribution for $\tilde{Y}(t)$. This is the key to understanding the physical meaning of the time-warping function, which will be explained later.

[14] Equation (8) implies that the transformation does not change the magnitude of the curve, but the curve is stretched at different rates determined by percentile function $X(\tau)$. Note that the mapping from $(t, \tilde{Y}[t])$ to $(X[\tau], Y[\tau])$ in (7) and (8) is nonunique in the sense that different types of transformation $\Phi_{\tilde{Y}}$ will map to a different pair of $(X[\tau], Y[\tau])$. However, once the function $\Phi_{\tilde{Y}}(t)$ is chosen, the mapping is uniquely defined.

[15] For each individual observed curve $\tilde{Y}_m(t)$, $m = \overline{1, M}$, $\Phi_{\tilde{Y}_m}(t)$ can be calculated from (6), the time-warping transformation function $X_m(\tau)$ is determined by the inverse of $\Phi_{\tilde{Y}_m}(t)$ as $X_m(\tau) = \Phi_{\tilde{Y}_m}^{-1}(\tau)$, and the new curve in the time-warped space is $Y_m(\tau) = \tilde{Y}_m(X_m[\tau])$.

[16] Figure 2 illustrates how two observed curves (red and blue curves) are converted to curves in the warped time space. The two observed curves have a single peak but differ in both their amplitudes and positions in the time axis (Figure 2a). If we want to find the "average" of these two curves, it may not be appropriate to take the arithmetic average of two curves directly because the direct average will yield a two-peak curve (the green curve in Figure 2a), which has a different pattern from the two original curves. To compute the functional average, we first compute the forward time transformation functions $\Phi_{\tilde{Y}_m}(t)$, shown in Figure 2b, which are the integral curves of the original curves, normalized by the total area under the original curves. As stated previously, the forward transformation functions $\Phi_{\tilde{Y}_m}(t)$ are cumulative breakthrough curves. The time-warping transformation functions $X(\tau)$ are depicted in Figure 2c, which are the inverse of curves in Figure 2b. The converted curves (amplitude) are shown in Figure 2d, where two curves have been aligned in the time axis. The dashed line segments in these plots demonstrate how the final curves in the time-warped space in Figure 2d are obtained. For $\forall\tau \in [0, 1]$, say $\tau = 0.4$, one first locates the corresponding $t = 9.0$ for the first curve from $X_1(\tau)$ in Figure 2c (or equivalently from $\Phi_1[t]$ in Figure 2b), then finds the value of $\tilde{Y}_1(9.0) = 0.18$ from Figure 2a, and finally assigns this value to $Y_1(0.4) = 0.18$. This procedure can be implemented efficiently.

2.2. Mean Curve

[17] It is worth noting from $\tilde{Y}(t) = Y(X^{-1}[t])$ in (3) that $\tilde{Y}(t)$ is a stochastic function itself with an argument that is also a stochastic process. To derive the sample mean curve, we denote $u = X^{-1}(t)$ and expand the equation at $\langle u\rangle$ using a Taylor expansion up to the first order [*Lu and Zhang*, 2003b]

$$\tilde{Y}(t) = Y(X^{-1}[t]) = Y(u) = Y(\langle u\rangle) + \left.\frac{dY}{du}\right|_{\langle u\rangle} u' + \left.\frac{d^2Y}{du^2}\right|_{\langle u\rangle} (u')^2 \tag{9}$$

or equivalently in terms of X:

$$\tilde{Y}(t) = Y(\langle u\rangle) + \left.\frac{dY}{dX}\right|_{\langle X\rangle} X' + \left.\frac{d^2Y}{dX^2}\right|_{\langle X\rangle} (X')^2. \tag{10}$$

We define the functional mean as the ensemble mean of the first term in (10),

$$\langle\tilde{Y}(t)\rangle_{\oplus} = \langle Y(\langle X^{-1}(t)\rangle)\rangle, \tag{11}$$

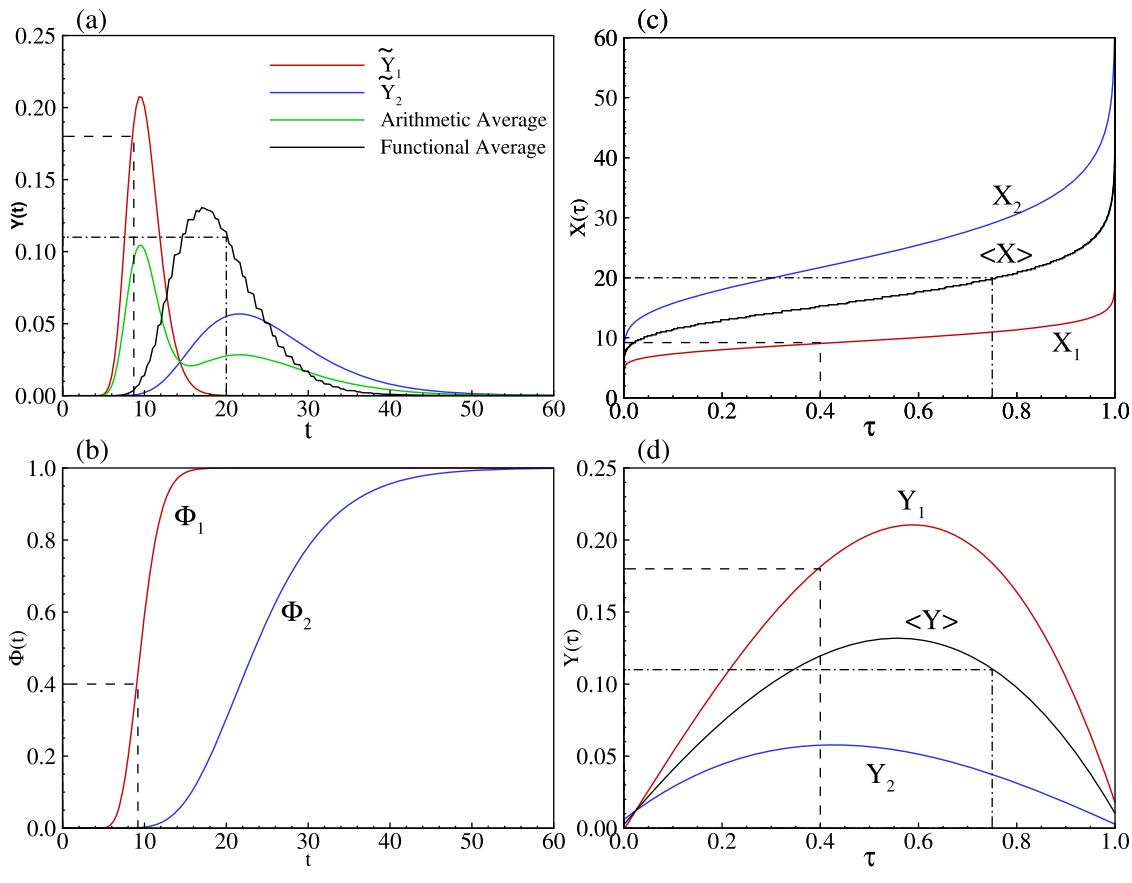

Figure 2. An example illustrating the procedure of finding functional average curve: (a) two original curves; (b) transformation function $\Phi(t)$; (c) time-warping transformation function $X(\tau)$, and (d) transformed curves $Y(\tau)$ in time-warped space. The arithmetic average and functional averages are also compared in Figure 1a.

where the symbol $\oplus$ stands for functional averaging. It has been shown [*Liu and Muller*, 2004] that the functional average $\langle \tilde{Y}(t) \rangle_{\oplus}$ has the smallest total deviation to sampled curves, if the square of distance is defined as,

$$d_{\oplus}^2(\tilde{Y}_1, \tilde{Y}_2) = \int_0^1 (X_1[\tau] - X_2[\tau])^2 d\tau + \int_0^1 (Y_1[\tau] - Y_2[\tau])^2 d\tau, \tag{12}$$

where $\tilde{Y}_1$ and $\tilde{Y}_2$ are two sampled curves, and $(X_1[\tau], Y_1[\tau])$ and $(X_2[\tau], Y_2[\tau])$ are their corresponding curves in the time-warped space.

[18] It should be emphasized that taking the ensemble mean of (9) or (10) will yield the arithmetic mean, just as taking the ensemble mean of hydraulic conductivity $K_s = e^f$ in the above example leads to the arithmetic mean $K_A = \langle K_s \rangle = e^{\langle f \rangle + \sigma_f^2/2}$, while the first-order approximation of $\langle K_s \rangle$ is $K_G = e^{\langle f \rangle}$.

[19] To find the functional mean curve, we first find the means of the curves in the time-warped space $\langle X(\tau) \rangle$ and $\langle Y(\tau) \rangle$. As discussed earlier, any pair of $(X[\tau], Y[\tau])$ in the time-warped space uniquely defines a curve in the original time space. So the mean curve in the original time space can be determined from $(\langle X(\tau) \rangle, \langle Y(\tau) \rangle)$ using (11). To estimate the ensemble means of $X(\tau)$ and $Y(\tau)$, one maps all observed curves $(t, \tilde{Y}_m[t])$, $m = \overline{1, M}$, to their corresponding curves in the warped time space as $(X_m[\tau], Y_m[\tau])$, $m = \overline{1, M}$, and then takes the arithmetic average:

$$\langle X(\tau) \rangle \approx \overline{X}(\tau) = \frac{1}{M} \sum_{m=1}^{M} X_m(\tau); \quad \langle Y(\tau) \rangle \approx \overline{Y}(\tau) = \frac{1}{M} \sum_{m=1}^{M} Y_m(\tau), \tag{13}$$

where the bars over the variables represent sample averaging, and $1/M$ may be replaced by other weights for important MCS sampling. This step is analogous to computing the arithmetic mean of the log-transformed values $\langle f \rangle = (1/M) \sum_{i=1}^{M} f_i$ in the example in calculating the mean hydraulic conductivity. The functional mean $\langle \tilde{Y}(t) \rangle_{\oplus}$ can be approximated by

$$\overline{\tilde{Y}}_{\oplus}(t) = \overline{Y}([\overline{X}^{-1}(t)]). \tag{14}$$

[20] In our example shown in Figure 2, the average of the curves in the time-warped space is calculated using the arithmetic average for both the amplitude and time-warping function (see Figures 2c and 2d). The dash-dotted segments illustrate how the mean curve (black curve) in Figure 2a is determined. For $\forall t \in [0, 60]$, say $t = 20$ (Figure 2a), one first finds the warped time τ from the time-warp function $\langle X \rangle$ in Figure 2c, $\tau = 0.75$ in this case, finds $\langle Y(0.75) \rangle = 0.11$ from Figure 2d, and then assigns this value to $\overline{\tilde{Y}}_{\oplus}(20) = 0.11$ in Figure 2a. Like the original curves, the functional average of the two curves has a single peak, and thus is physically more reasonable.

[21] We should emphasize that the essence of the functional averaging is that different observed curves are transformed using different mapping functions. As stated above, the magnitude of the curve does not change at all during the mapping process. Therefore, if one uses the same mapping function $\Phi(t)$ (thus, the same $X[\tau]$) for all curves, it is equivalent to stretching all curves in the same way. It is easy to show that

$$\begin{aligned} \overline{\tilde{Y}}_{\oplus}(t) &= \overline{Y}(\overline{X}^{-1}[t]) = \frac{1}{M} \sum_{i=1}^{M} Y_i(\overline{X}^{-1}[t]) \\ &= \frac{1}{M} \sum_{i=1}^{M} \tilde{Y}_i(X[X^{-1}\{t\}]) = \overline{\tilde{Y}}(t). \end{aligned} \tag{15}$$

Here we used the relationships $Y_i(\tau) = \tilde{Y}_i(X[\tau])$ and $\overline{X}^{-1}(t) = X^{-1}(t)$ in this particular case. This equation indicates that using the same mapping function for all observed curves will result in the arithmetic average. Intuitively, if one stretches all curves the same way, computes the mean curve from the stretched curves, and then shrinks the mean curve back, the final mean curve will be the same as the mean curve calculated directly from the original observed curves.

[22] What is the physical meaning of this functional average? Recall that each $X_i(\tau)$ is the percentile function of the travel time distribution corresponding to curve $\tilde{Y}_i(t)$. For any $\tau_0 \in [0, 1]$, $X_i(\tau_0)$ is the $(100\tau_0)$th percentile of its travel time distribution of $\tilde{Y}_i(t)$, and $Y_i(\tau_0) = \tilde{Y}_i(X_i[\tau_0])$ is the probability density at the $(100\tau_0)$th percentile. Therefore, the arithmetic average $\overline{X}(\tau_0)$ is the average of times (over all realizations) that represent the same $(100\tau_0)$th percentile in the original curves, while $\overline{Y}(\tau_0)$ is the average of probability density at the times that have the percentile $100\tau_0$. In other words, both averages $\overline{X}(\tau)$ and $\overline{Y}(\tau)$ are computed based on the percentile.

[23] The functional average can provide information that may be lost by traditional arithmetic averaging. Such cases include times when the functional average peak concentrations are higher than the arithmetic average concentrations, especially when the increase in concentration leads to crossing of a dose threshold. Another instance where the functional average is useful is in system-level modeling where breakthroughs are carried forward to represent groundwater contributions to part of a larger calculation. In such instances, one might want a representative curve to use to do simple preliminary analysis with, and using either the median or functional average would better represent the expected system behavior of the groundwater component of the system model. Finally, we note that the functional average contains information that can be used to calculate average travel times using inverse methods, whereas the arithmetic mean cannot be used in such a fashion. Thus, the functional average provides an additional metric that can be used to characterize the breakthrough behavior in combination with more traditional median and arithmetic average curves.

[24] Again, we use the example shown in Figure 2 to illustrate the idea of the percentile average. The percentile functions X_1 and X_2 in this example are depicted in Figure 3b. For any fixed percentile, say the 40th percentile as indicated in the figure, the times corresponding to this percentile can be read from Figure 3b as $X_1(0.4) = 9.0$ and $X_2(0.4) = 21.6$, respectively, which yields the average $\overline{X}(0.4) = 15.3$. The magnitude of the functional mean at

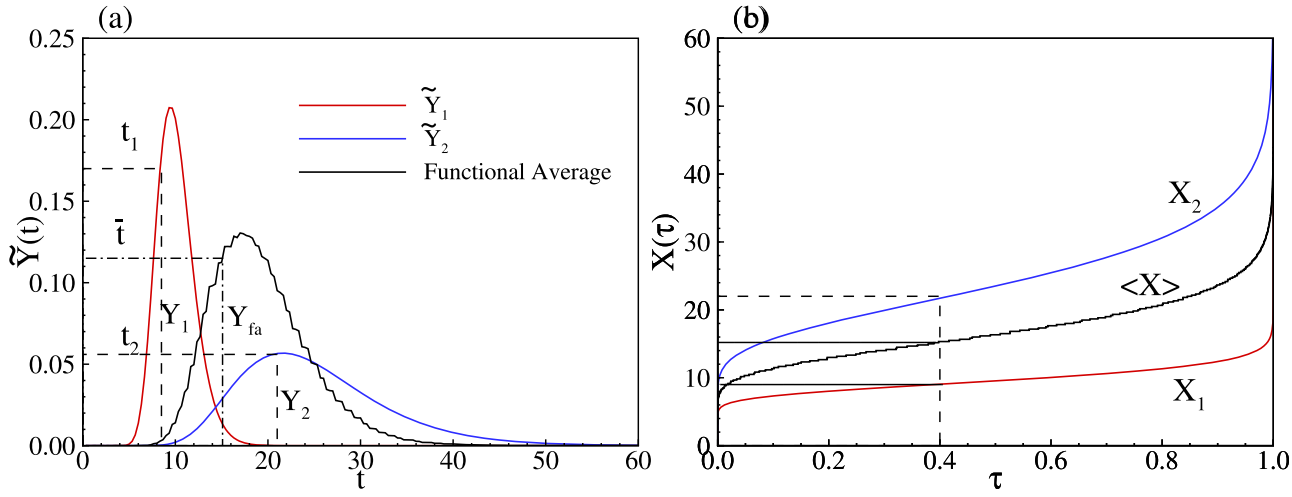

Figure 3. An example illustrating the concept of the percentile averaging: (a) two original curves; (b) time-warping transformation function $X(\tau)$.

$t = 15.3$, $\overline{\tilde{Y}}(15.3)_{\oplus} = 0.113$, is then computed by the average of $\tilde{Y}_1(9.0) = 0.17$ and $\tilde{Y}_2(21.6) = 0.056$.

[25] In many transport models, breakthrough curves were derived by the particle-tracking method. Suppose we run M simulations, N particles are released in each simulation, and T_{ij} denotes the travel time for the j-th fastest particle reaching a compliance boundary in the i-th simulation. For convenience, we assume that for any given i, T_{ij}, $j = \overline{1,N}$, are distinct, i.e., $T_{ij} < T_{ik}$ for $j < k$. Each particle's arrival contributes $100/N$ percentile. In this discrete case, percentile averaging is equivalent to ranking averaging of particles, i.e., an averaging of travel time over all fastest particles, second fastest particles, and so on. One computes the average of the j-th fastest particle over all M model runs $\overline{T}_{\bullet j} = (1/M)\sum_{i=1}^{M} T_{ij}$, and then the percentile average breakthrough curve can be constructed from the histogram of $\overline{T}_{\bullet j}, j = \overline{1,N}$.

2.3. Uncertainty of the Sample Mean Curve

[26] Although the unknown population mean curve is not a random curve, the sample mean curve is a random curve that depends on a finite number of sampled curves. It has been shown that the functional sample mean is pointwise asymptotically normal [*Liu and Muller*, 2004]:

$$\sqrt{M}\left(\overline{\tilde{Y}}(t) - \langle \tilde{Y}(t)\rangle_{\oplus}\right) \to \varepsilon(t), \tag{16}$$

where $\varepsilon(t)$ follows a normal distribution with zero mean and a variance to be determined later.

[27] Subtracting (11) from (10) and ignoring the second-order term yields an equation for perturbation of $\tilde{Y}(t)$:

$$\tilde{Y}'(t) = Y'(\langle u\rangle) + \left.\frac{dY}{dX}\right|_{\langle X\rangle} X', \tag{17}$$

from which one derives the variance

$$\hat{\sigma}^2_{\tilde{Y}}(t) = \hat{\sigma}^2_{YY}(\langle u\rangle) + 2\left.\frac{dY}{dX}\right|_{\langle X\rangle}\hat{\sigma}^2_{XY}(\langle u\rangle) + \left[\left.\frac{dY}{dX}\right|_{\langle X\rangle}\right]^2 \hat{\sigma}^2_{XX}(\langle u\rangle), \tag{18}$$

where $\langle u\rangle = \langle X(t)\rangle^{-1}$. It can be shown that this equation is equivalent to (35) of *Liu and Muller* [2004], but here it is derived concisely from the perturbation approach. The one-point covariances $\hat{\sigma}^2_{XX}$, $\hat{\sigma}^2_{YY}$, and $\hat{\sigma}^2_{XY}$ are defined in the time-warped space and calculated as,

$$\hat{\sigma}^2_{XX}(\tau) = \frac{1}{M-1}\sum_{m=1}^{M}(X_m[\tau] - \overline{X}[\tau])^2, \tag{19}$$

$$\hat{\sigma}^2_{YY}(\tau) = \frac{1}{M-1}\sum_{m=1}^{M}(Y_m[\tau] - \overline{Y}[\tau])^2, \quad \sqrt{a^2+b^2}, \tag{20}$$

$$\hat{\sigma}^2_{XY}(\tau) = \frac{1}{M-1}\sum_{m=1}^{M}(X_m[\tau] - \overline{X}[\tau])(Y_m[\tau] - \overline{Y}[\tau]). \tag{21}$$

These definitions are slightly different from those by *Liu and Muller* [2004], in which $\overline{X}_m(\tau) = (1/m)\sum_{i=1}^{m} X_i$ and $\overline{Y}_m(\tau) = (1/m)\sum_{i=1}^{m} Y_i$ are used instead of sample means $\overline{X}(\tau)$ and $\overline{Y}(\tau)$. When the number of samples is large, such differences only have a very small impact on the results. The confidence interval of the functional sample mean can be constructed as [*Liu and Muller*, 2004],

$$\left[\overline{\tilde{Y}}_{\oplus}(t) - \Phi^{-1}(1-\alpha/2)\sqrt{\hat{\sigma}^2_{\tilde{Y}}(t)/M},\ \overline{\tilde{Y}}_{\oplus}(t) + \Phi^{-1}(1-\alpha/2)\sqrt{\hat{\sigma}^2_{\tilde{Y}}(t)/M}\right], \tag{22}$$

where Φ is the cumulative probability function of the standard normal distribution, and α is the level of desired confidence.

3. Numerical Implementation

[28] For a given set of sampled curves $\tilde{Y}_m$, $m = \overline{1,M}$, the numerical implementation for calculating the functional or percentile average can be outlined as follows:

[29] 1. Interpolate original curves $\tilde{Y}_m(t)$, $m = \overline{1, M}$, if needed, such that all curves have values at the same observation points t_i, $i = \overline{1, N}$.

[30] 2. Calculate the normalized curve and the forward transformation function $\Phi_{\tilde{Y}_m}(t)$, $m = \overline{1, M}$, using (5) and (6). Note that $\Phi_{\tilde{Y}_m}(t)$ has a range of [0, 1].

[31] 3. Compute functions $X_m(\tau)$ by numerical inverse of $\Phi_{\tilde{Y}_m}(t)$. This is done by finely discretizing the domain [0, 1] into N_p segments τ, $0 = \tau_0 < \tau_1 < \cdots < \tau_{N_p} = 1$, and for each τ_i finding an index k such that $\tau_i > \Phi_{\tilde{Y}_m}(t_k)$ and $\tau_i \leq \Phi_{\tilde{Y}_m}(t_{k+1})$. The value of t_k is then assigned to $X_m(\tau_i) = t_k$.

[32] 4. Determine functions $Y_m(\tau)$ by assigning $Y_m(\tau_i) = \tilde{Y}_m(t_k)$, $i = \overline{1, N_p}$, where t_k has been determined in the previous step.

[33] 5. Calculate means $\langle X(\tau_i) \rangle$ and $\langle Y(\tau_i) \rangle$, $i = \overline{1, N_p}$, in the time-warped space using $X_m(\tau_i)$ and $Y_m(\tau_i)$, $m = \overline{1, M}$.

[34] 6. Evaluate the functional average $\overline{\tilde{Y}}_{\oplus}(t_j) = \langle Y(\tau_k) \rangle$, where k is such an index that $t_j > \langle X(\tau_k) \rangle$ and $t_j \leq \langle X(\tau_{k+1}) \rangle$.

[35] 7. For instantaneous BTCs, one may need to scale the functional average curve such that the area under the curve is one.

[36] 8. Compute (co)variances σ^2_{XX}, σ^2_{YY}, and σ^2_{XY} using (19)–(21), and construct the confidence interval using (22).

4. Application to Breakthrough Curves From Field-Scale Simulations

[37] Breakthrough curves used in this example were created during particle transport modeling for calculations done in support of the Material Disposal Area (MDA) G performance assessment (PA) [*Stauffer et al.*, 2005b]. MDA G has been in operation since 1957 and is currently the only active low-level waste repository at Los Alamos National Laboratory (LANL). Since its initial operation, radioactive waste generated at the laboratory has been disposed of in pits and shafts on the mesa top. Particle transport simulations are used to estimate conservative species breakthrough times as mass travels from the base of the waste through the unsaturated zone, into the water table aquifer, and finally to a compliance boundary that is a vertical plane normal to the direction of groundwater flow that lies 100 m downgradient from the disposal site boundary. The numerical model of the site is composed of a variable resolution 3-D finite-element mesh with rock strata defined from a detailed geologic framework model [*Stauffer et al.*, 2005b]. Particles spend most of their travel time in the rhyolitic Bandelier Tuff that forms the upper 60 m of the mesa at MDA G.

[38] For the current analysis we examine uncertainty in breakthrough related to uncertainty in four different stratigraphic units of the Bandelier Tuff including three units of the Tshirege Member (Qbt2, Qbt1v, Qbt1g) and the Otowi Member (Qbo). More information on the geology of these rocks can be found in the work of *Stauffer et al.* [2005a] and references therein. The following hydrologic properties in these units are considered as piecewise random functions: the saturated hydraulic conductivity K_s, the pore size distribution parameter α, the van Genuchten fitting parameter n, the saturated water content θ_s, and residual water content θ_r. The assumption on parameter distributions is consistent with field observations [*Springer*, 2005]. Rock properties at the site have relatively large variability. In particular, large variability on the pore size distribution parameter α and fitting parameter n will have a significant effect on flow and solute transport [*Lu and Zhang*, 2002].

[39] The realizations of rock properties are generated using the Latin hypercube sampling (LHS) method [*McKay et al.*, 1979]. This method is commonly used to reduce the number of runs necessary for MCS to achieve a reasonably accurate random distribution. For each realization, we first create a steady state flow simulation with 1 mm yr^{-1} background infiltration over the surface of the 3-D model, followed by a transport simulation, using the convolution-based particle tracking (CBPT) method [*Robinson et al.*, 2010] implemented in finite element heat- and mass-transfer code (FEHM) [*Zyvoloski et al.*, 1997]. The CBPT method was developed to simulate resident or flux-averaged solute concentrations in groundwater models. The method is valid for steady state flow and linear transport processes such as sorption with a linear sorption isotherm, diffusion into matrix rock, and first-order decay. The method combines a deterministic component to treat advection and a random-walk component to simulate dispersion.

[40] There may some other sources (besides the uncertain rock properties) that contribute to the uncertainty of the breakthrough curve, such as reconstruction of concentration breakthrough curves from a discrete number of particles [*Fernez-Garcia and Sanchez-Vila*, 2011]. In each simulation, 15,625 particles were uniformly released in a 1 m cube at a depth corresponding to the waste burial depth near the center of the site. The effect of the total particle number has been checked visually to make sure that the breakthrough curves appear to be meaningful. The number of particles reaching the compliance boundary plane as a function of time are used to determine the breakthrough curves. Four quantities of interest (5th and 95th percentiles, mean, and median breakthroughs) from 1000 realizations were examined to assess the convergence of these realizations. The study indicated that these four quantities from 100 realizations are very close to those from 1000 realizations, indicating that 100 LHS realizations are approaching convergence to the 1000 LHS Monte Carlo simulations, and that 1000 realizations are sufficient to achieve the convergence.

[41] The breakthrough curves from 1000 realizations are shown in Figure 4a. It is seen from the figure that there is a large variability on these breakthrough curves because of large variations on hydraulic properties. The difference between these BTCs can be larger than one order of magnitude on the time axis. In several realizations, the particles move so slowly that only a small portion of particles reach the water table at 200,000 yr. These realizations have a significant impact on the moments of the breakthrough curves. It should be noted that, except for several curves mentioned above, the area under each individual breakthrough should be one, although it appears that the areas for different curves are different because of the log scale on the time axis.

[42] Some of the statistics are plotted in Figure 4b. These statistics include direct arithmetic average (labeled as *mean* in the figure), 5 percentile, 50 percentile (median), and 95

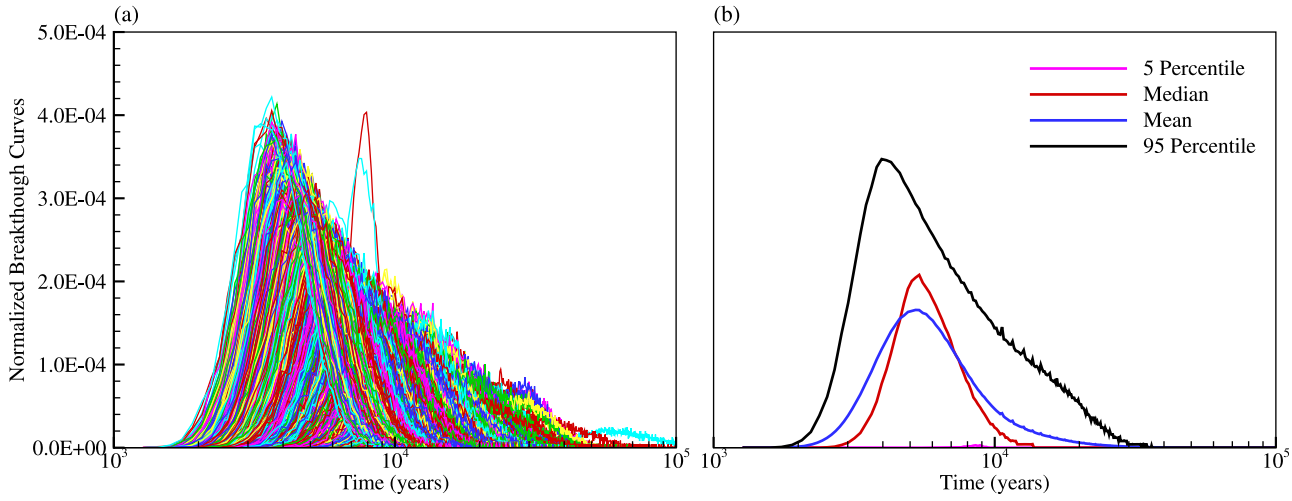

Figure 4. (a) Breakthrough curves derived from transport simulations using 1000 realizations of hydrologic properties, and (b) statistics of these curves: median curve, arithmetically averaged curve, 5-, and 95-percentile curves.

percentile. For any point at the time axis, the direct arithmetic average was computed by averaging (vertically) over all of the curves. The percentile curves were derived by connecting their percentile value among 1000 values at all time t_i, $i = \overline{1, N}$. For example, at each time t_i, one finds the median among all 1000 values at this time, and then connects the median values from all times, which is the median curve. Note that the arithmetic average and these percentiles may not coincide with any particular breakthrough curve. The results confirm the conclusion from our previous study that the median curve performs better than the mean curve in reducing earlier arrival and long tailing [*Stauffer and Lu*, 2012].

[43] Now we apply percentile averaging to 1000 breakthrough curves. For each curve $(t, \tilde{Y}_m[t])$, the forward transformation function $\Phi_{\tilde{Y}_m}$ is computed from (6), which is the cumulative breakthrough and also a cumulative distribution function. As an example, Figure 5a shows 20 out of 1000 transformation functions or cumulative distribution functions. The time-warping functions (Figure 5b) are their inverse $X_m(\tau) = \Phi^{-1}_{\tilde{Y}_m}$. We should emphasize again that the time-warping function $X_m(\tau)$ is the percentile function. The amplitude $Y_m(\tau)$ is determined from $Y_m(\tau) = \tilde{Y}_m(X_m[\tau])$. The sample mean of time-warping functions is also depicted in Figure 5b. In the time-warped space, all (amplitude) curves are aligned (not shown). The sample means of $X(\tau)$ and $Y(\tau)$ are computed from all 1000 samples and they are used to derive the mean curve in the original time space. The mean breakthrough curve from the percentile average is compared with other curve statistics in Figure 6. Compared to the arithmetic mean curve, the percentile mean has a large, early arrival time and a short tailing.

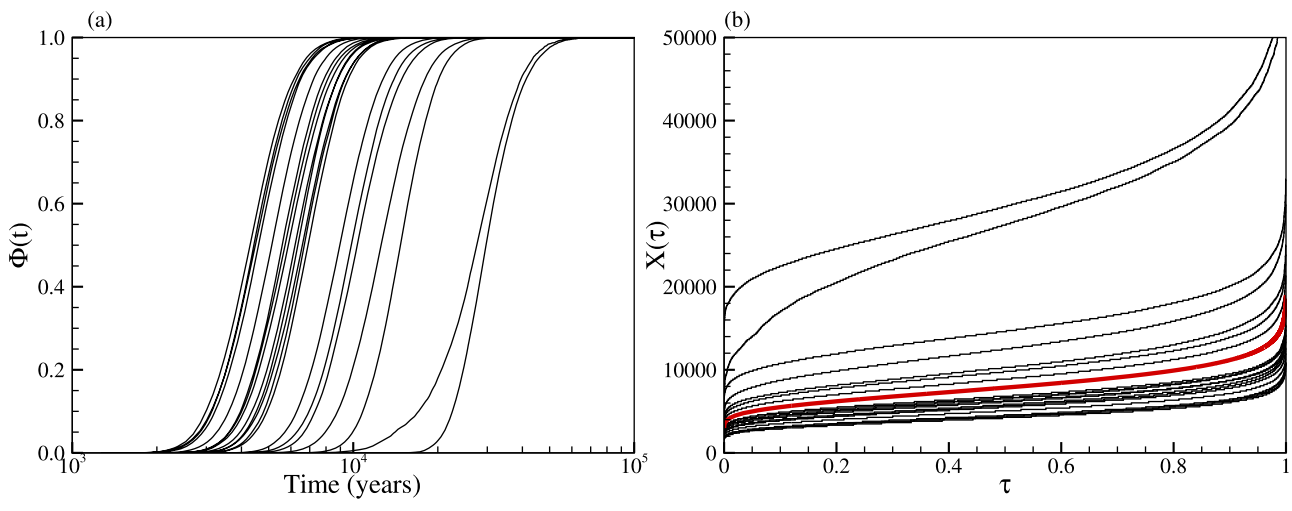

Figure 5. (a) Twenty out of 1000 forward transformations (cumulative distribution functions) and (b) their time-warping functions (percentile functions). The sampling average of 1000 percentile functions is also shown (thick curve).

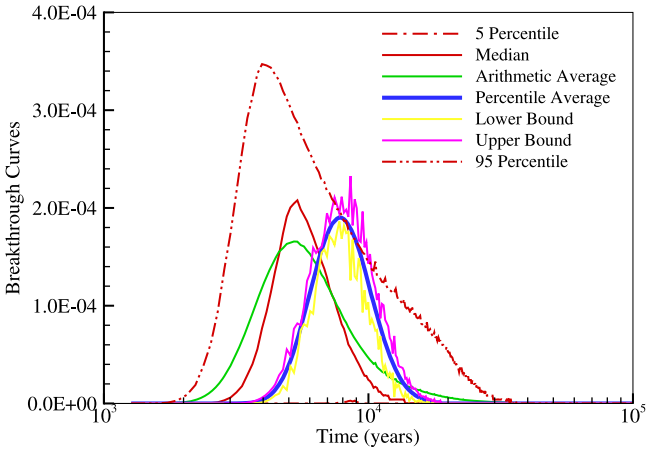

Figure 6. Comparison of various averages of the breakthrough curves from Monte Carlo simulations.

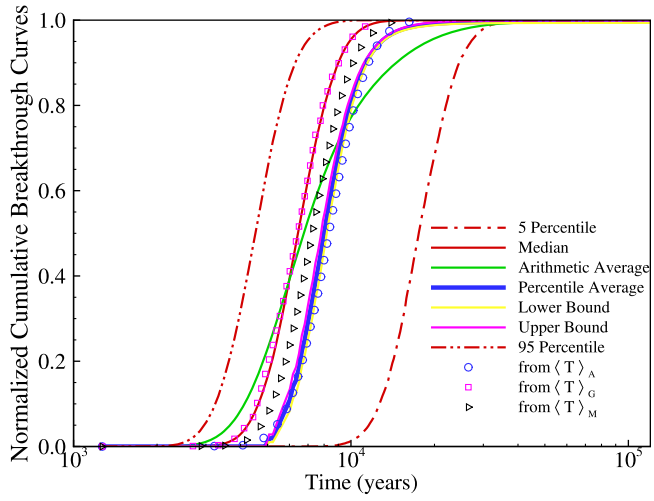

Figure 7. Comparison of various averages of the cumulative breakthrough curves from Monte Carlo simulations.

More importantly, the arithmetic mean averaging may underestimate the peak mass flow rate.

[44] The confidence interval (upper and lower bounds) of the sample mean curve with a confidence level of 0.95 is also shown in Figure 6. It should be noted that the confidence interval of the sample mean curve is different from the confidence interval of the Monte Carlo BTCs. The latter can be constructed using the sample mean curve plus/minus a few standard deviations (only if the distribution is normal, which is not the case for BTCs), or constructed using percentiles (such as 2.5 and 97.5 percentiles) of Monte Carlo BTCs. This is widely used for BTC analysis, and then most of the BTC realizations will fall into this confidence interval, provided that the confidence interval was constructed from a sufficiently large number of realizations. However, in our approach, we are trying to find the average of any number of BTCs (such as two curves in Figure 1), and we may not have enough curves to determine the confidence interval that will envelope most of curves. Instead, we provide a confidence interval for the sample mean curve, which means that, if one takes another set of realizations with the same sample size and computes the functional average curve, at the probability of 0.95, the sample mean curve will fall in the confidence interval given in the figure. This confidence interval of the sample mean curve is different from that for the Monte Carlo BTCs in that both the lower and upper bounds of the confidence interval for the sample mean curve are functions of the number of realizations, and therefore does not require a large number of realizations to construct the interval. For example, if one only has a small number of realizations, the interval will be much wider and as the number of realizations increases, the interval will become narrow and eventually the upper and the lower bounds will overlap. From the statistical point of view, the sample mean curve follows a normal distribution and therefore the confidence interval can be constructed by plus/minus a few standard errors (depending on the desired accuracy) to the sample mean curve, as indicated in equation (22).

[45] We can also apply the percentile averaging method to cumulative breakthrough curves. Figure 7 compares various statistics of cumulative BTCs, including some conventional curve statistics: the arithmetic mean, 5th-, 50th-, and 95th-percentile curves, percentile mean curve and its upper and lower bounds, as well as several other curves that will be explained later.

[46] It is seen from Figure 7 that the percentile mean curve of the cumulative breakthrough curves is very similar in shape to most of the individual curves from MCS, while again the arithmetic average has a different shape with nearly all sampled BTCs (not shown). Comparing to the percentile average, the arithmetic average has an earlier first-arrival time and a longer tailing. The median curve (50th percentile), and the 5th- and 95th-percentile curves are also plotted in the figure.

[47] Several other curves in Figure 7 are derived differently, where the 5th and 95th percentiles are percentile curves for Monte Carlo BTCs; lower and upper bounds represent the bounds for percentile average; $\langle T \rangle_A$, $\langle T \rangle_G$, and $\langle T \rangle_M$ stand for the breakthrough curves created from arithmetic, geometric, and median travel time, respectively. Since any instantaneous BTC represents the time distribution of particles arriving at the compliance boundary, for any fixed value on the vertical axis of cumulative BTCs, say 0.5, we can determine the travel time for each BTC realization and then the probability distribution of travel time from 1000 realizations. As expected, χ^2 goodness-of-fit tests indicated that the travel time follows lognormal distributions (not shown). One can also compute statistics of these travel times for any fixed value of the vertical axis, in particular, the arithmetic mean, the geometric mean, and the median of these travel times. From each of these statistics, we can construct one breakthrough curve. For instance, for each fixed value on the vertical axis, we calculate the arithmetic average of travel times derived from 1000 BTC realizations, and reconstruct one BTC using the arithmetic mean for all (discrete) values on the vertical axis. The BTCs derived from this approach are compared in Figure 7. It is noted that the BTC created from the arithmetic mean travel time is nearly identical to the percentile average of cumulative BTCs.

[48] It is easy to see that the percentile average curve derived from instantaneous BTCs is consistent with the mean curve (circles in Figure 7, labeled as $\langle T \rangle_A$) constructed from the arithmetic averaging of BTCs at any fixed cumulative mass (vertical axis). This is due to the fact that, the mean mass flow rate at any time t_0 (or percentile p_0) on the percentile mean curve of BTC realizations is the arithmetic average of the mass flow rates at time t_i, $i = \overline{1, 1000}$, that stands for the same percentile p_0 on the i-th BTC, and that any fixed value p $(0 \leq p \leq 1)$ on the vertical axis of the normalized cumulative BTC is equivalent to the $(100p)$th percentile on its corresponding (instantaneous) BTC.

5. Conclusions and Discussions

[49] In this paper, we derived the functional mean and its confidence interval for random curves using a combination of the time-warping and perturbation approach. One important feature of the functional mean is its variance-minimizing property. This methodology can be applied to any set of random curves. In particular, for (instantaneous) breakthrough curves generated from Monte Carlo transport simulations, we recognize that the forward transformation function $\Phi(t)$ is the normalized cumulative breakthrough curve and it is also a cumulative distribution function of the travel time, and that the time-warping function $X(\tau)$, which is the inverse of the forward transformation function, is a quantile (or percentile) function. The arithmetic average of these time-warping functions for all BTC realizations in the time-warped space indicates that our functional average in this case is, in fact, a percentile averaging. Under this time-warping function, the magnitude functions of breakthrough curves are completely aligned. By percentile averaging, we mean that the breakthrough curves are averaged not at the actual time, as in calculating the traditional mean breakthrough curve, but at the times that represent the same percentile in these BTC realizations. Since the normalized cumulative breakthrough curve is a cumulative distribution function of travel time, percentile averaging of the (instantaneous) breakthrough curves is equivalent to taking the average of cumulative breakthrough curves over any fixed normalized cumulative mass (the vertical axis of the plot for the cumulative breakthrough curves). As the result, the most convenient way to compute the percentile mean BTC is by taking the average of the cumulative BTCs according to the same percent of mass arriving at the compliance boundary.

[50] The applicability of the approach was demonstrated using BTCs created from Monte Carlo simulations of particle transport in the Bandelier Tuff at MDA G, Los Alamos, where five parameters in four stratigraphic units are considered as random parameters that follow some prescribed probability distributions.

[51] Comparing to the arithmetic mean breakthrough curve, the functional mean breakthrough curve has several advantages. The functional mean breakthrough resembles most of the individual BTC realizations, while the arithmetic mean breakthrough has a different shape with those BTC realizations. In addition, the functional mean breakthrough is not very sensitive to outliers. The arithmetic mean breakthrough curve in general overestimates the mass flow rate at earlier time and late time but underestimates the peak mass flow rate at intermediate time. More importantly, it may underestimate the peak mass flow rate, which may be very critical for some applications.

[52] Potentially, the time-warping technique may be extended to some other applications in hydrology, such as computing particles' mean trajectory in particle-tracking transport simulations, or evaluating statistics of concentration fields created from Monte Carlo simulations.

[53] **Acknowledgment.** This work was supported by Environmental Programs at Los Alamos National Laboratory.

References

Bektas, S., and Y. Sisman (2010), The comparison of L_1 and L_2-norm minimization methods, *Int. J. Phys. Sci.*, *5*(11), 1721–1727.

Dai, Z., A. Wolfsberg, Z. Lu, and H. Deng (2009), Scale dependence of sorption coefficients for contaminant transport in saturated fractured rock, *Geophys. Res. Lett.*, *36*, L01403, doi:10.1029/2008GL036516.

Fernez-Garcia, D., and X. Sanchez-Vila (2011), Optimal reconstruction of concentrations, gradients and reaction rates from particle distributions, *J. Contam. Hydrol.*, *121–122*, 99–114.

Gasser, Th., H. G. Muller, W. Kohler, L. Molinari, and A. Prader (1984), Nonparametric regression analysis of growth curves, *Ann. Stat.*, *12*, 210–229.

Govindaraju, R. S., and B. S. Das (2007), *Moment Analysis for Subsurface Hydrologic Applications*, 292 pp., Springer, Dordrecht, Netherlands.

Hu, B. X., J. Wu, and C. He (2004), On stochastic modeling of groundwater flow and solute transport in multi-scale heterogeneous formations, *Comput. Appl. Math.*, *23*(2–3), 121–151.

Kneip, A., and Th. Gasser (1992), Statistical tools to analyze data representing a sample of curves, *Ann. Stat.*, *16*, 82–112.

Lin, Z., and D. Li (2007), Asymptotic normality for L_1-norm kernel estimator of conditional median under association dependence, *J. Multivariate Analysis*, *98*, 1214–1230.

Liu, X., and H.-G. Muller (2004), Functional convex averaging and synchronization for time-warped random curves, *J. Am. Stat. Assoc.*, *99*(467), 687–699.

Lu, Z., and D. Zhang (2002), Stochastic analysis of transient flow in heterogeneous variably saturated porous media: The van Genuchten-Mualem constitutive model, *Vadose Zone J. 1*, 137–149.

Lu, Z., and D. Zhang (2003a), On importance sampling Monte Carlo approach to flow and transport in heterogeneous geological formations, *Adv. Water Resour.*, *26*(11), 1177–1188.

Lu, Z., and D. Zhang (2003b), Solute spreading in nonstationary flows in bounded heterogeneous saturated-unsaturated media, *Water Resour. Res.*, *39*(3), 1049, doi:10.1029/2001WR000908.

McKay, M. D., R. J. Beckman, and W. J. Conover (1979), A comparison of three methods for selecting values of input variables in the analysis of output from a computer code, *Technometrics*, *21*(2), 239–245, doi:10.2307/1268522.

Pan, F., M. Ye, J. Zhu, Y. S. Wu, B. X. Hu, and Z. Yu (2009), Incorporating layer- and local-scale heterogeneities in numerical simulation of unsaturated flow and tracer transport, *J. Contam. Hydrol.*, *103*, 194–205.

Riva, M. A., D. Guadagnini, X. Fernandez-Garcia, X. Sanchez-Vila, and Th. Ptak (2008), Relative importance of geostatistical and transport models in describing heavily tailed breakthrough curves at the Lauswiesen site, *J. Contam. Hydrol.*, *101*, 1–13.

Robinson, B. A., G. Srinivasan, and Z. Dash (2010), A particle tracking transport method for the simulation of resident and flux-averaged concentration of solute plumes in groundwater models, *Comput. Geosci.*, *14*(4), 779–792.

Silverman, B. W. (1995), Incorporating parametric effects into functional principal components analysis, *J. R. Stat. Soc. Ser. B*, *57*, 673–689.

Springer, E. P. (2005), Statistical exploration of matrix hydrologic properties for the Bandelier Tuff, Los Alamos, New Mexico, *Vadose Zone J.*, *4*, 505–521.

Stauffer, P. H., and Z. Lu (2012), Quantifying transport uncertainty in unsaturated rock using Monte Carlo sampling of retention curves, *Vadose Zone J.*, in press.

Stauffer, P. H., K. H. Birdsell, M. S. Witkowski, and J. K. Hopkins (2005a), Vadose zone transport of 1,1,l-Trichloroethane: Conceptual model validation through numerical simulation, *Vadose Zone J.*, *4*, 760–773.

Stauffer, P. H., H. S. Viswanathan, B. A. Robinson, C. W. Gable, G. L. Cole, D. E. Broxton, E. P. Springer, and T. G. Schofield (2005b), Groundwater Pathway Model for the Los Alamos National Laboratory Technical Area 54, Material Disposal Area G, *Los Alamos National Laboratory, document LA-UR-05-7393*, 66 pp., Los Alamos Natl. Lab., Los Alamos, N. M.

Wang, K., and Th. Gasser (1997), Alignment of curves by dynamic time warping, *Ann. Stat.*, *25*, 1251–1276.

Wang, K., and Th. Gasser (1999), Synchronizing sample curves nonparametrically, *Ann. Stat.*, *27*, 439–460.

Zhang, Y., D. A. Benson, and B. Baeumer (2007), Predicting the tails of breakthrough curve in regional-scale alluvial systems, *Ground Water*, *45*(4), 473–484.

Zyvoloski, G. A., B. A. Robinson, Z. V. Dash, and L. L. Trease (1997), Summary of the models and methods for the FEHM application: A finite element heat- and mass-transfer code, *LA-13307-MS*, Los Alamos Natl. Lab., Los Alamos, N. M.

Z. Lu and P. H. Stauffer, Computational Earth Sciences Group (EES-16), Los Alamos National Laboratory, MS T003, Los Alamos, NM 87545, USA. (zhiming@lanl.gov)